

Systemic physiology augmented functional near-infrared spectroscopy hyperscanning: a first evaluation investigating entrainment of spontaneous activity of brain and body physiology between subjects

Sabino Guglielmini[Ⓢ],^{a,*} Gino Bopp,^a Valentine L. Marcar[Ⓢ],^{a,b}
Felix Scholkmann[Ⓢ],^{a,c,§} and Martin Wolf[Ⓢ],^{a,§}

^aUniversity of Zurich, University Hospital Zurich, Department of Neonatology,
Biomedical Optics Research Laboratory, Zurich, Switzerland

^bUniversity Hospital Zürich, Comprehensive Cancer Center Zürich, Zürich, Switzerland

^cUniversity of Bern, Institute of Complementary and Integrative Medicine, Bern,
Switzerland

Abstract

Significance: Functional near-infrared spectroscopy (fNIRS) enables measuring the brain activity of two subjects while they interact, i.e., the hyperscanning approach.

Aim: In our exploratory study, we extended classical fNIRS hyperscanning by adding systemic physiological measures to obtain systemic physiology augmented fNIRS (SPA-fNIRS) hyperscanning while blocking and not blocking the visual communication between the subjects. This approach enables access brain-to-brain, brain-to-body, and body-to-body coupling between the subjects simultaneously.

Approach: Twenty-four pairs of subjects participated in the experiment. The paradigm consisted of two subjects that sat in front of each other and had their eyes closed for 10 min, followed by a phase of 10 min where they made eye contact. Brain and body activity was measured continuously by SPA-fNIRS.

Results: Our study shows that making eye contact for a prolonged time causes significant changes in brain-to-brain, brain-to-body, and body-to-body coupling, indicating that eye contact is followed by entrainment of the physiology between subjects. Subjects that knew each other generally showed a larger trend to change between the two conditions.

Conclusions: The main point of this study is to introduce a new framework to investigate brain-to-brain, body-to-body, and brain-to-body coupling through a simple social experimental paradigm. The study revealed that eye contact leads to significant synchronization of spontaneous activity of the brain and body physiology. Our study is the first that employed the SPA-fNIRS approach and showed its usefulness to investigate complex interpersonal physiological changes.

© The Authors. Published by SPIE under a Creative Commons Attribution 4.0 International License. Distribution or reproduction of this work in whole or in part requires full attribution of the original publication, including its DOI. [DOI: 10.1117/1.NPh.9.2.026601]

Keywords: hyperscanning; functional near-infrared spectroscopy; interpersonal brain synchronization; eye contact; cross-brain coherence; systemic physiology augmented functional near-infrared spectroscopy hyperscanning; systemic physiology augmented functional near-infrared spectroscopy; SPA-fNIRS.

Paper 21063TNRR received Nov. 5, 2021; accepted for publication Mar. 18, 2022; published online Apr. 18, 2022.

*Address all correspondence to Sabino Guglielmini, Sabino.Guglielmini@usz.ch

§Shared last authorship.

1 Introduction

Humans are a social species that engage in complex interactions during goal-oriented cooperation.¹ Social cognition is the basis for such interactions and includes three main components: simulation, empathy, and mentalization. The standard simulation notion refers to a functional process in which an observer tries to voluntarily reproduce, even with the help of imagination, the same mental states of another individual.² First, social cognition has been attributed by Gallese³ to an embodied simulation enabling an immediate understanding and associated with mirror neuron systems, i.e., neuronal systems that are activated when an intentional action is performed (such as motor action) and when the observing the same action. Studies have shown activation of the motor cortex in 6-month-old children when observing actions.^{4,5} The second component is empathy, which is defined as the ability to share feelings and emotions.⁶ It is automatic, different for everyone and it is stronger depending on the type of relationship one has with the observed person.^{7,8} Third, mentalization is an essential part of social cognition and the ability to read the state of mind, such as desires, beliefs, and intentions in others.^{9–11}

Past research has focused on establishing the link between behavior and brain activity of single subjects outside of real social interactions.^{12–14} Subsequent research studied individual brain activity during simulated social situations.¹⁵ Most studies about social cognition were performed considering an interpersonal relationship only from a purely social point of view. Some time ago it was already pointed out that the neurobiology of human social behavior is an important, but neglected research topic that requires more attention than it has attracted so far.¹⁶ Today it is possible to measure brain activity of two interacting subjects simultaneously, a technique referred to as hyperscanning.^{17–23} It is a well-established methodology for studying individuals during natural interactions²⁴ and has been used in various contexts over a number of years. It allows monitor of both emotional^{25,26} and cognitive aspects^{27–29} of social interaction.

Several neuroimaging techniques have been adopted for hyperscanning, each with its advantages and disadvantages. Hyperscanning experiments were originally performed with electroencephalography (EEG) and it is still the technique that is used the most.^{30–34} While functional magnetic resonance imaging (fMRI) is probably the most prominent neuroimaging technology, it requires the subjects to enter a highly constrained space in the scanner and does not allow investigating social interactions in a naturalistic environment. The scanner generates loud noise likely to entrain rhythms in any physiological parameter. In contrast, functional near-infrared spectroscopy (fNIRS) is a noninvasive optical neuroimaging method that enables cortical brain activity to be measured in everyday situations and natural settings.^{35,36} fNIRS indirectly measures brain activity based on optical absorption changes in the brain tissue associated with changes in cerebral tissue oxygenation and hemodynamics, i.e., concentration changes of oxyhemoglobin ($[O_2Hb]$), deoxyhemoglobin ($[HHb]$), and total hemoglobin ($[tHb]$).³⁷ Our research group was one of the first to demonstrate the feasibility to use fNIRS for human hyperscanning studies.^{27,38,39}

As demonstrated by Hamilton,⁴⁰ properly studying social interactions “requires studying the brain and bodily coordination together” since “interacting brains exist within interacting bodies.” We adopted this concept. The measurement of brain-to-brain coupling needs to be accompanied by the measurement of body-to-body coupling and body-to-brain coupling. In our view, this is important for two reasons. First, it allows investigating intrasubject (within a subject) as well as intersubject (between subjects) body–brain interactions. Second, it enables to investigate how much systemic physiology impacts the fNIRS signals measured on the head. This is of particular importance since parameters measured by fNIRS are influenced by systemic physiology,^{41,42} e.g., changes in blood pressure^{43,44} and the concentration of CO_2 in the blood.^{45,46} We investigated this aspect in detail in the last years and developed the methodology appropriate to measure and analyze fNIRS signals along with systemic physiological signals, which we termed “systemic physiology augmented fNIRS” (SPA-fNIRS).^{47–49} This approach has not yet been applied to hyperscanning which allows the introduction of a new methodology: SPA-fNIRS hyperscanning.

In our exploratory study, the primary interest was to propose a new framework enabling the investigation of interbody and interpersonal neural synchrony in any form of interaction between pairs of subjects. We employed SPA-fNIRS hyperscanning to capture intersubject brain-to-brain, brain-to-body, and body-to-body coupling during goal-oriented interaction while blocking and not blocking the visual communication between the subjects. To this end, the differences in the

coupling strength were compared between a resting-state condition where the subjects were not looking at each other, and a condition where they were looking at each other. We hypothesized that the coupling of the signals between pairs is higher when they make eye contact compared with the condition when the visual communication channel is blocked.

2 Materials and Methods

2.1 Participants

27 pairs of healthy adults (mean age: 32.1 years, age range: 18 to 65 years, 24 males, and 30 females) participated in the study. None of them reported neurological, psychiatric or other diseases that might affect the results of our study. Due to the lack of optical coupling between the optodes caused by the dense hair of two participants, two pairs were excluded from the analysis. In addition, another dataset was excluded because the electrocardiogram electrodes in one participant were disconnected during the measurement. Thus, from 27 pairs, 24 were considered in the analysis. This study was approved by the Ethics Committee of the County of Zurich (ethics approval code KEK-ZH-Nr. E50/2002). All participants were informed about the experimental procedure and provided their informed, written consent. All participants were remunerated for participating in the study. The relation between the two individuals was assessed and categorized as familiar (siblings, spouses and boyfriends/girlfriends) or unfamiliar. The familiar group consisted of eight pairs of siblings and six couples (spouses and boy/girlfriends), while the unfamiliar group was composed of five colleagues pairs and five strangers pairs. The new guidelines for conducting and reporting fNIRS studies were taken into account.⁵⁰

2.2 Data Acquisition and Experimental Paradigm

Changes in $[O_2Hb]$, $[HHb]$, and $[tHb]$ were measured on the head by optical neuroimaging with fNIRS (NIRSport, Berlin, Germany). The system provided 16-long-distance channels (30 mm), and 8-short-distance channels (8 mm) using the two wavelengths (760 and 850 nm). The sampling frequency was set to 7.81 Hz. Optodes were positioned according to the 10-20 system using individually sized caps (NIRx Medizintechnik GmbH, Berlin, Germany). Figure 1(c) depicts the sensitivity map highlighting the ability of the setup to measure the prefrontal cortex as well as the left and right frontotemporal cortex. The short distance channels were employed to capture changes in the superficial (extracerebral) tissue compartment.^{51,52}

In addition, systemic physiology was measured by the following 11 parameters: heart rate (HR), mean arterial blood pressure (MAP), pulse pressure (PP), systolic blood pressure (SBP), diastolic blood pressure (DBP), arterial oxygenation (SpO_2), electrodermal activity (EDA), skin temperature (Temp) on the left and right wrist, and end-tidal carbon dioxide ($P_{ET}CO_2$). HR, MAP, PP, SBP, DBP, and SpO_2 were acquired with the SOMNOtouch™ NIBP device (SOMNO Medics, Germany) at a sampling rate of 4 Hz, EDA and skin temperature with the E4 wristbands (Empatica, Boston, Massachusetts, United States) at 4 Hz, and $P_{ET}CO_2$ with a capnograph (Nonin Life Sense; Nonin Medical, Plymouth, Minnesota, United States) at 1 Hz. Figure 1(a) shows the measurement setup.

Paired participants were instructed to adopt comfortable posture on a chair and rested their heads on the backrest to reduce head movement. They were seated in front of each other on opposite sides of a table [Fig. 1(a)] at a distance of 180 cm.

A measurement session lasted 21 min. The experimental protocol was divided into two phases. In the first phase, no interaction between the subjects took place and they kept their eyes closed for 11 min. In the second phase, they looked at each other for 10 min. The first minute of the measurement (prebaseline) was discarded from the analysis with the aim of ensuring that the participants were settled and the measurement free of initial, task-unrelated changes [Fig. 1(b)].

Given the difficulty of maintaining eye contact for the entire duration of the second phase, participants were instructed to maintain eye contact for as long as possible and, in case of discomfort, to look at the other participant's body and then focus on his/her eyes again. During the experiment, pairs were asked not to talk and minimize the movement of their head to prevent motion artifacts.

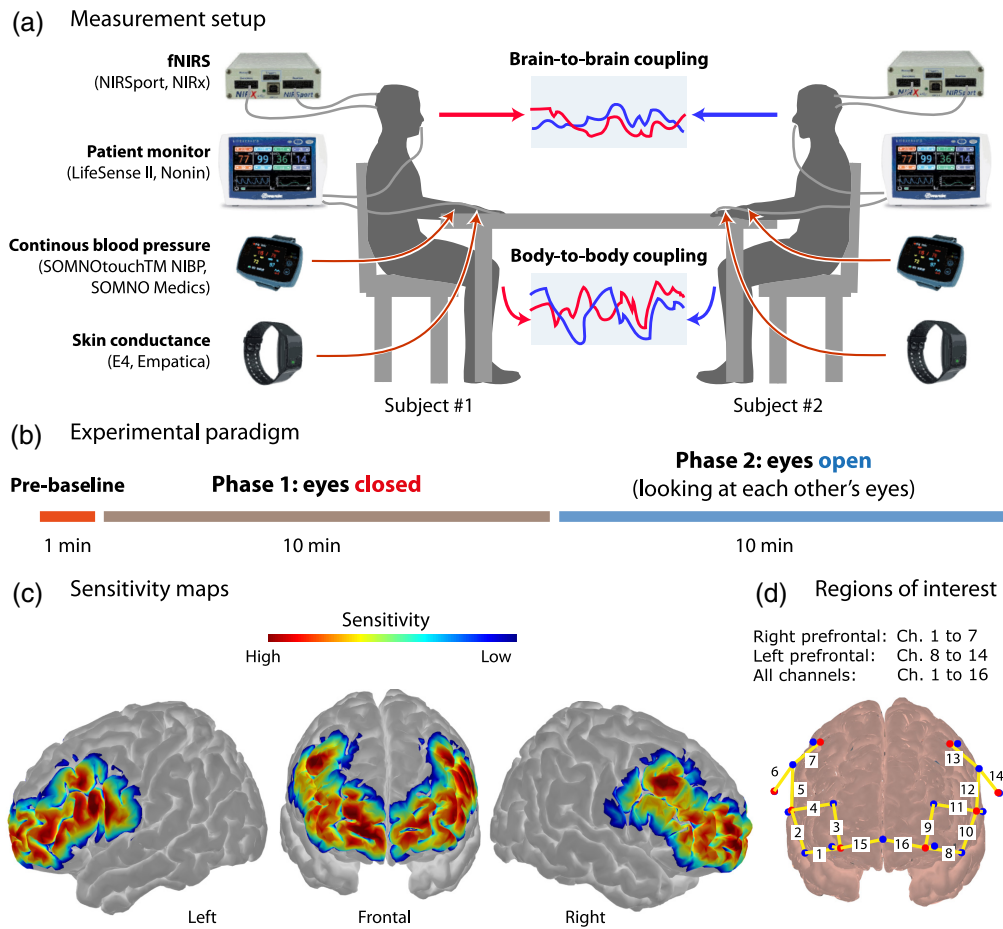


Fig. 1 Experimental design. (a) Measurement setup. Participants sit in front of each other; (b) the two task conditions and the timeline for each experiment; (c) sensitivity maps generated with the Monte Carlo photon transport software for the depicted channel arrangement; (d) probe with the legend of the three ROIs.

2.3 Signal Preprocessing

fNIRS data were preprocessed and analyzed applying the HOMER2 (version 2.2) package and customized routines in MATLAB® (The MathWorks, Inc., Natick, Massachusetts, United States).

Short channel regression was performed to remove extracerebral hemodynamics to increase the sensitivity of the fNIRS measurement to deeper tissue layers, ideally to neurovascular coupling.⁵³ To this end, a MATLAB® function implemented by NIRx Medical Technologies was utilized based on Saager and Berger⁵⁴ and Scholkmann et al.⁵⁵

Optical density time series were converted to $[O_2Hb]$, $[HHb]$, and $[tHb]$ time series by the modified Beer–Lambert law⁵⁶ using HOMER2 routines (hmrIntensity2OD, hmrSSR, and hmrOD2Conc) assuming a fixed differential path-length factor of 6.⁵⁷ The absorption coefficients were calculated based on the extinction coefficients from Kollias and Gratzer.⁵⁸

In our analysis, we also considered fNIRS signals without applying short channel regression ($[O_2Hb]$ (raw), $[HHb]$ (raw), $[tHb]$ (raw)) to investigate the impact of short channel regression on the results. Some fNIRS time series had to be excluded from further analysis due to an insufficient signal-to-noise ratio. The exclusion was performed based on the coefficients of variation (CV). Time series with a CV above 7.5%⁵⁹ were excluded from the successive fNIRS analysis due to insufficient data quality. All data were screened visually for movement artifacts. No relevant artifacts were found. Based on the location of the optodes [see Fig. 1(d)], three regions of interest (ROI) were determined: the left, right, and the entire prefrontal region of the head.

The channels belonging to the same ROI were averaged. As a result, 18 fNIRS signals were obtained: [O₂Hb], [HHb], and [tHb] (i) of the left prefrontal region ([O₂Hb] (left), [HHb] (left), [tHb] (left)), [O₂Hb] (left, raw), [HHb] (left, raw), and [tHb] (left, raw)), (ii) of the right prefrontal region ([O₂Hb] (right), [HHb] (right), [tHb] (right)), [O₂Hb] (right, raw), [HHb] (right, raw), and [tHb] (right, raw)), (iii) and all channels ([O₂Hb] (left + right), [HHb] (left + right), [tHb] (left + right)), [O₂Hb] (left + right, raw), [HHb] (left + right, raw), and [tHb] (left + right, raw)). The fNIRS time series of each experiment were then synchronized to the systemic physiological time series.

2.4 Data Analysis

The time- and frequency-dependent correlation between the time series was determined for each type of signal and pair of participants using the wavelet transform coherence (WTC) analysis.⁶⁰ Figure 2 provides an example of fNIRS and systemic physiological signals with the corresponding WTC analysis results. For each pair of time series, we considered the mean of the coherence calculated for four frequency bands: very low-frequency band (VLF, 0.002 to 0.08 Hz), low-frequency band 1 (LF1, 0.015 to 0.15 Hz), low-frequency band 2 (LF2, 0.08 to 0.15 Hz), and heart rate band (HR, 1 to 2 Hz). Thus, four WTC time series for each of the 29 pairs of time series were obtained.

For each dyad, the WTC between the same pair of time series was calculated [Figs. 3(a) and 3(b)]. Then, for each of the four frequency bands [Fig. 3(c)], the median of the coherence values was calculated, leading to one time-dependent WTC signal [Fig. 3(d)] for each pair of time series. This resulted in $(29 \times 4) - 1$ time-dependent WTC signals for each dyad, where the -1 represents the absence of the P_{ET}CO₂ time series in the HR frequency band as illustrated in the bottom right plot in Fig. 2. The coherence values outside the cone of influence were excluded from the further WTC analyses.

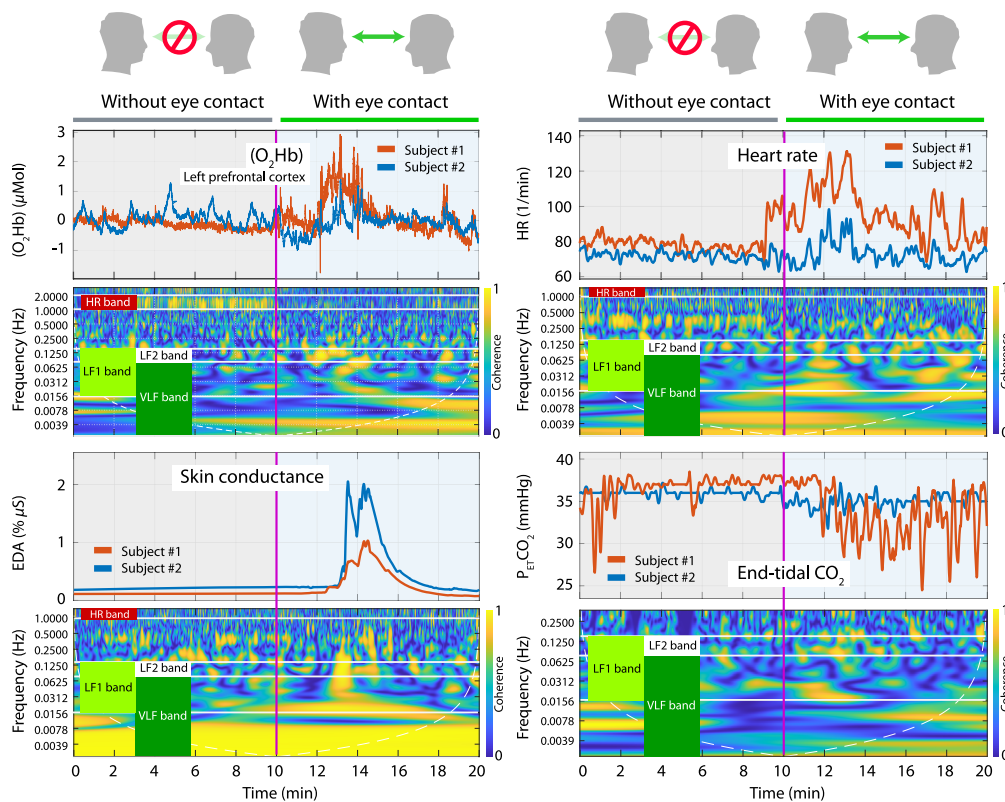


Fig. 2 Illustrative example of physiological and fNIRS time series of one pair and the respective wavelet coherence. The figure shows the four frequency bands that have been taken into account in the analysis.

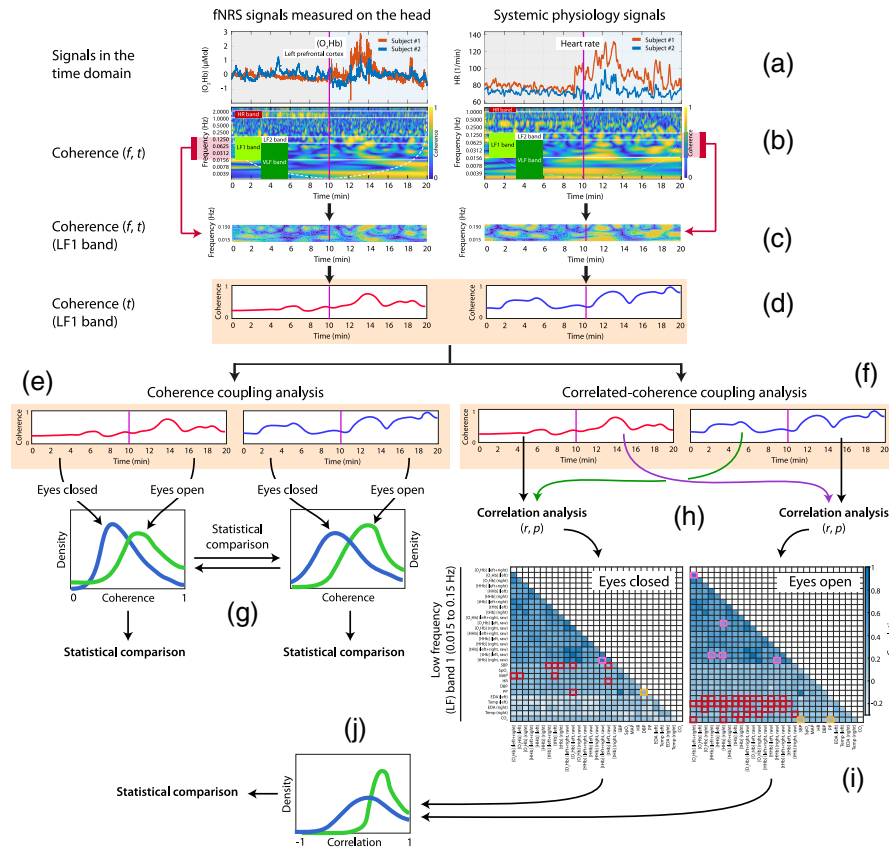


Fig. 3 Visualization of the signal processing and data analysis steps of the coherence and correlated-coherence coupling analysis. The figure shows the steps performed in the analysis for a given dyad taking as an example, a pair of fNIRS signals ($[O_2Hb]$ (left)) and the HR of the two participants (a) considering only the LF1 band. (b) The wavelet coherence analysis of the two pairs of time series is performed and the respective scalograms are shown with the four frequency bands. (c) One frequency band is selected and (d) the median of the coherence values is calculated, leading to two time-dependent WTC signals. (e) In the coherence coupling analysis, the time-dependent coherence of the fNIRS and systemic physiology signals have been averaged over the two conditions. (g) The ART ANOVA was then performed on the resulting coherence values to assess any difference between the eyes-closed and eye-contact conditions. (f) In the correlated-coherence coupling analysis, the time-dependent coherence signals are split according to the two conditions and (h) Spearman correlation and its significance levels are calculated, (i) leading to a correlation matrix of the correlation coefficients from all types of time series. (j) Finally, the correlation distribution of each type of time series over the two conditions was tested with Kolmogorov–Smirnov test.

In our analysis, we only investigated the coupling between subjects, not within a subject, since the focus of our study was to investigate the coupling between subjects, i.e., the brain-to-brain, brain-to-body, and body-to-body coupling.

2.4.1 Coherence coupling analysis

The time-dependent coherence of the fNIRS and systemic physiology time series was averaged over the two conditions. Thus, for each frequency band we obtained two coherence values c_{SnEC} and c_{SnEO} , where Sn is one of the 29 possible WTC signals and indexes EC and EO indicate the eyes-closed and eyes-open conditions, respectively [Fig. 3(e)]. The aligned rank transformation analysis of variance (ART ANOVA),⁶¹ a nonparametric ANOVA, was performed to assess any difference between the two conditions [Fig. 3(g)]. In addition to the condition, also the group factor, consisting of two levels (familiar and unfamiliar pair) and the respective interaction (condition \times group) were evaluated. Finally, a false discovery rate (FDR) correction was applied to the p -values to correct the multiple comparison situation. This analysis was conducted in R .

As a control analysis, we calculated the WTC for each type of signal for 2400 random pairs with replacement. The WTC values obtained by this procedure were then averaged over the two conditions and the four frequency bands. For each type of signal and each frequency band, we compared the distribution of true WTC values with that obtained from the randomly shuffled pairs by performing the Wilcoxon rank-sum test. This analysis was performed to assess that the functional hyperconnectivity between pairs occurred because of social interaction.

2.4.2 Correlated-coherence coupling analysis

The correlation between each time-dependent WTC signal and the remaining 28 time-dependent WTC signals was evaluated [Fig. 3(b)]. The Spearman correlation (r) and the significance level (p -value) were calculated, generating a 28×28 matrix of WTC time-series correlation coefficients for each individual pair, each condition (eyes-closed and eye contact) and each frequency band [Fig. 3(i)].

Then, a group average was performed by calculating the median of all the individual correlation matrices, obtaining a single correlation matrix for each condition and frequency band, as

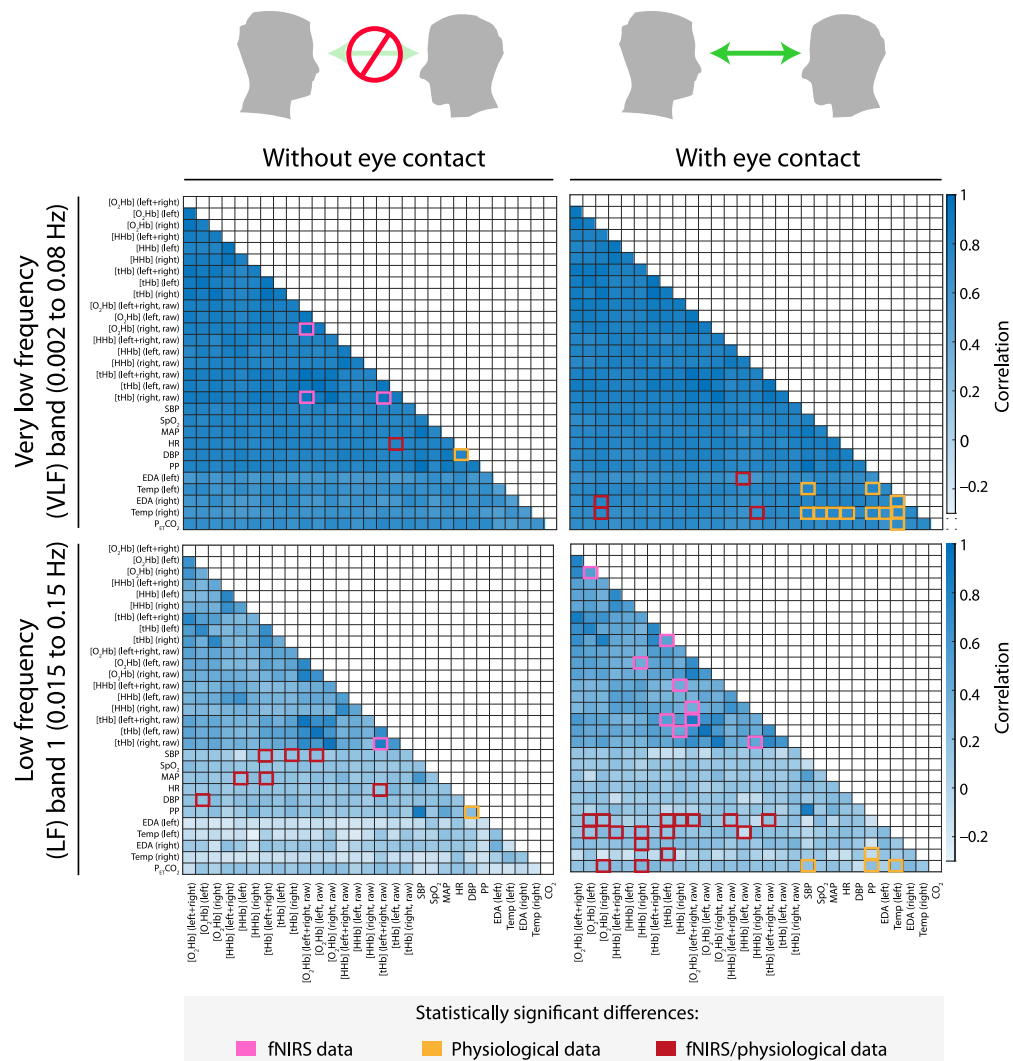


Fig. 4 Group averages of the correlation matrices comparing the eyes-closed and eyes-open conditions in the VLF band (top left and top right, respectively) and LF1 band (bottom left and bottom right, respectively). In the two frequency bands, a marked matrix value indicates a significant difference and a higher median of the distribution than the other condition of the respective frequency band.

illustrated in Figs. 4 and 5. For the group average, only correlation coefficients were used that were statistically significantly different from 0 ($p < 0.05$) to ensure that the group average was based only on meaningful physiological changes from the individual measurements.

To investigate whether the correlation distribution of each pair of time series during the eye-contact condition was statistically different from the one during the eyes-closed condition, in each frequency range the Kolmogorov–Smirnov test was performed [Fig. 3(j)]. The significant results are visualized in Figs. 6–8 separated into four bands (VLF, LF1, LF2, and HR) and three groups: fNIRS, systemic physiological and fNIRS/systemic physiological data.

In addition, the difference in the correlation distribution between familiar pairs and unfamiliar pairs groups was assessed. First, the difference of the correlation matrix values evaluated during the eye-contact condition and that during the eyes-closed condition for each of the four bands was computed. Next, a group average was performed by determining the median split for the familiar pairs and unfamiliar pairs as depicted in Figs. S1 and S2 in the [Supplemental Materials](#). The difference between the distributions of the two groups was finally evaluated by Kolmogorov–Smirnov test in each frequency range.

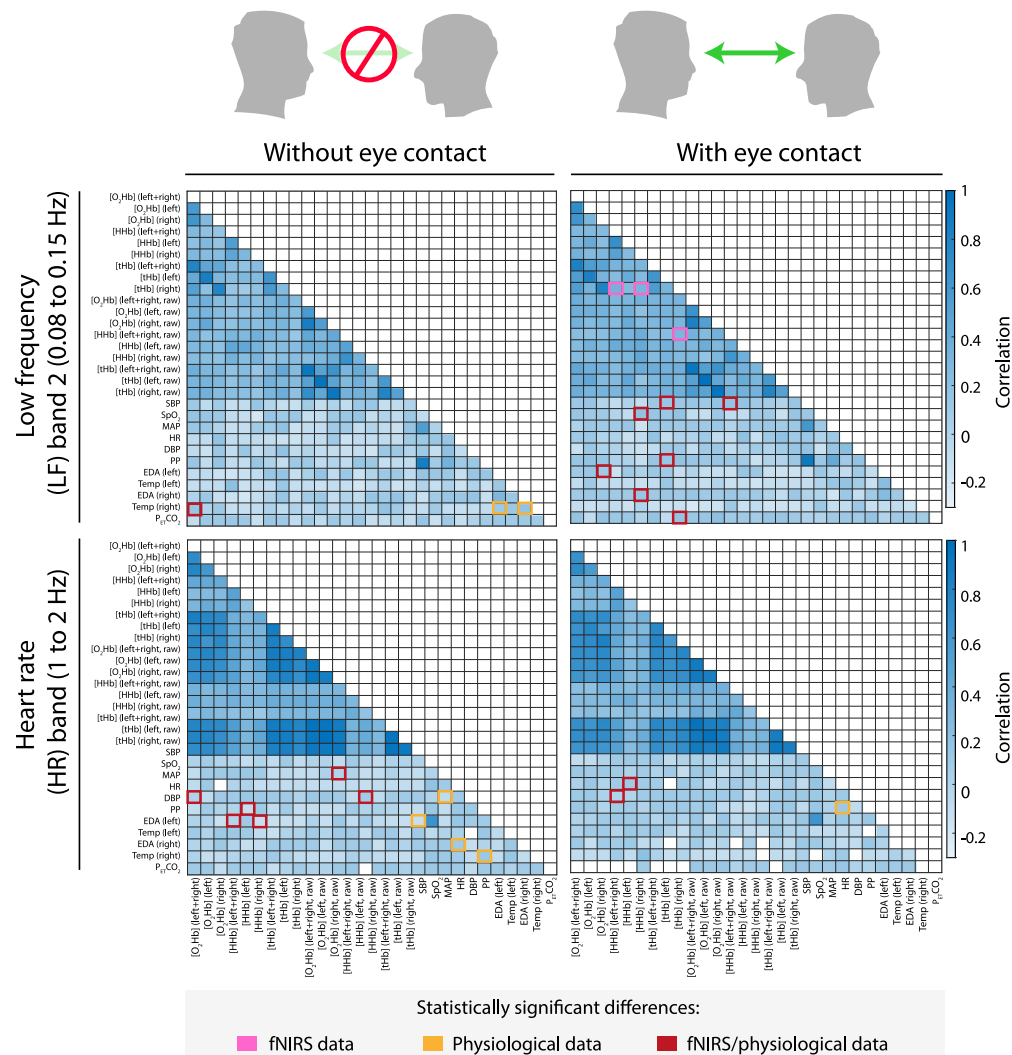


Fig. 5 Group averages of the correlation matrices comparing the eyes-closed and eyes-open conditions in the LF2 band (top left and top right, respectively) and HR frequency band (bottom left and bottom right, respectively). In the two frequency bands, a marked matrix value index indicates a significant difference and a higher median of the distribution than the other condition of the respective frequency band.

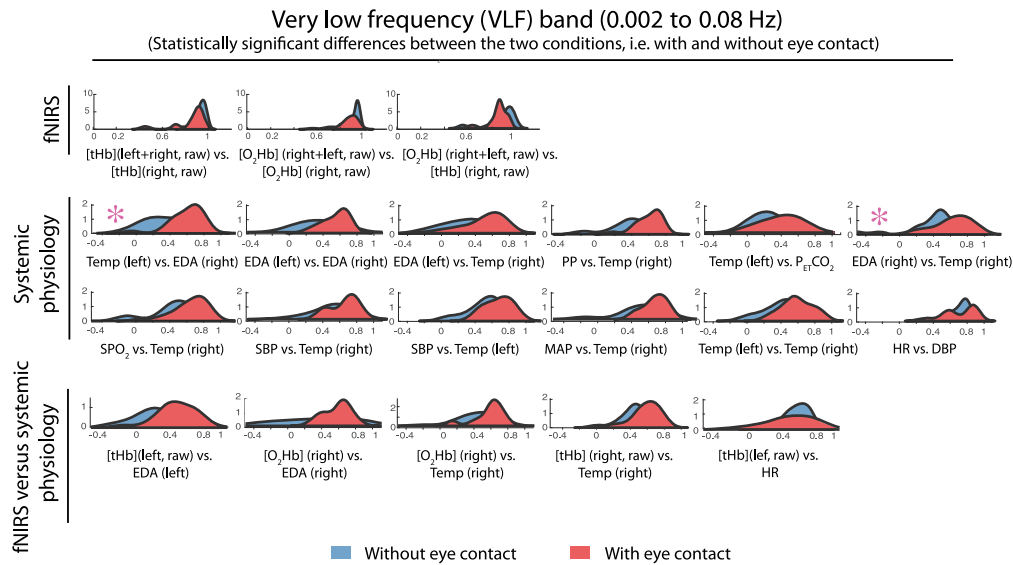


Fig. 6 Probability density functions of the distributions of each correlation coefficient of the 24 pairs in the VLF band separated into three groups: fNIRS, physiological, and fNIRS-physiological data. The probability density functions relative to the eye-contact condition are shown in red and those relative to the eyes-closed condition in blue. In the above figure are reported only the significant differences as a result of the Kolmogorov–Smirnov test. An asterisk indicates that the p -values are significant after the FDR correction.

3 Results

3.1 Coherence Coupling Analysis

3.1.1 Differences between eyes closed and open

The fNIRS results of the ART ANOVA are summarized in Table S1 in the [Supplemental Materials](#), and the systemic physiology results are summarized in Table S2 in the [Supplemental Materials](#).

Significant results related to the difference between the two conditions are illustrated in Fig. 9.

After performing an FDR correction, results showed a significant difference between the two conditions in [tHb] (left + right) (LF1 band, $p = 0.001$) (Table S1 in the [Supplemental Materials](#)), in Temp (left) and HR (VLF band, $p = 0.010$ and $p = 0.003$, respectively) (Table S2 in the [Supplemental Materials](#)). While both [tHb] (left + right) and HR showed a higher coherence in eye-contact condition compared with eyes-closed condition, Temp (left) presented an opposite effect (eye-contact coherence < eyes-closed coherence) (Fig. 9).

Additional significant coherence occurred without FDR correction where coherence during eye contact appeared higher in fNIRS signals in the VLF band, [O₂Hb] (left) ($p = 0.012$), [O₂Hb] (right) ($p = 0.043$), [O₂Hb] (left + right) ($p = 0.031$), and in the LF1 band, [O₂Hb] (right, raw) ($p = 0.017$), [O₂Hb] (left + right) ($p = 0.016$), [tHb] (right) ($p = 0.004$) as summarized in Table S1 in the [Supplemental Materials](#) and illustrated in Fig. 9. No difference was observed between the corrected fNIRS signals and those without applying the short channel regression.

Regarding the systemic physiology signals, EDA (left), in the HR band, and HR, in the LF1 band, showed a statistically higher coherence in the eye-contact condition compared with the other one ($p = 0.004$ and $p = 0.011$, respectively), while pairs exhibited a higher correlation in Temp (left) and Temp (right) signals when they were not looking at each other (LF1 band, $p = 0.010$ and $p = 0.041$, respectively) as listed in Table S2 in the [Supplemental Materials](#) and depicted in Fig. 9.

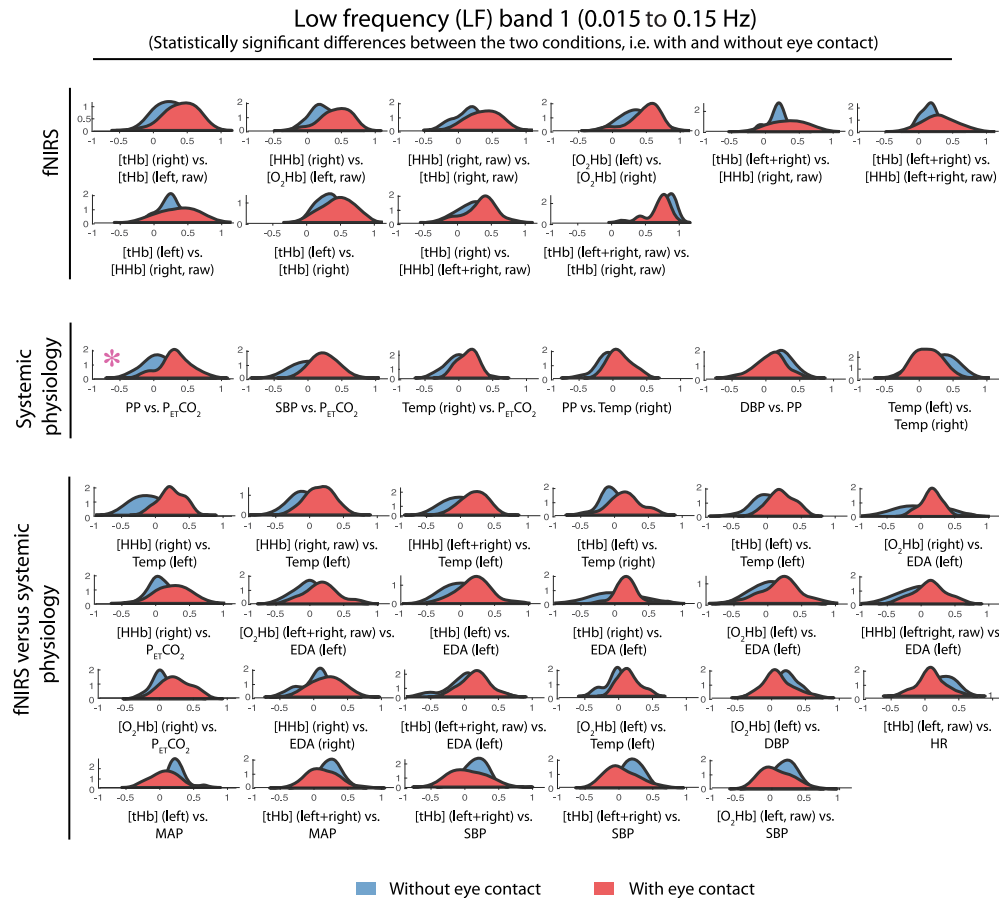


Fig. 7 Probability density functions of the distributions of each correlation coefficient of the 24 pairs in the LF1 band separated into three groups: fNIRS, physiological, and fNIRS-physiological data. The probability density functions relative to the eye-contact condition are shown in red and those relative to the eyes-closed condition in blue. In the above figure are reported only the significant differences as a result of the Kolmogorov–Smirnov test. An asterisk indicates that the p -values are significant after the FDR correction.

It is important to note that the outliers in the violin plots shown in Figs. 9–11 do not impact the results since ART ANOVA is based on ranks and therefore not affected by extreme values.

3.1.2 Impact of the type of relationship

The pairs who took part in our study belonged to two different groups according to their type of relationship: the first group included siblings and couples (spouses and boy/girlfriends) and the second pairs did not know each other or to a lesser extent than the other group.

After performing the FDR correction, our results showed that the coupling in the familiar pairs was higher than in the other group in the LF1 band for $[O_2Hb]$ (right, raw) ($p < 0.001$), $[tHb]$ (right, raw) ($p = 0.004$), HR ($p = 0.004$), and in VLF band for $[tHb]$ (left) ($p < 0.001$). On the contrary, in the case of $P_{ET}CO_2$ in the LF1 band, the correlation was found to be higher in unfamiliar pairs ($p = 0.004$). These results are reported in Tables S1 and S2 in the [Supplemental Materials](#) and are visualized in Fig. 10.

Without FDR correction, other significant differences in the coherence were noted. In all significant fNIRS results, the familiar pairs exhibited a higher hyperconnectivity. These fNIRS signals are $[O_2Hb]$ (right), $[tHb]$ (right), and $[tHb]$ (left + right) in the VLF band ($p = 0.014$, $p = 0.021$, and $p = 0.006$, respectively), $[O_2Hb]$ (left + right, raw) and $[tHb]$ (left + right) in the LF1 band ($p = 0.016$ and $p = 0.014$, respectively), and $[O_2Hb]$ (right, raw)

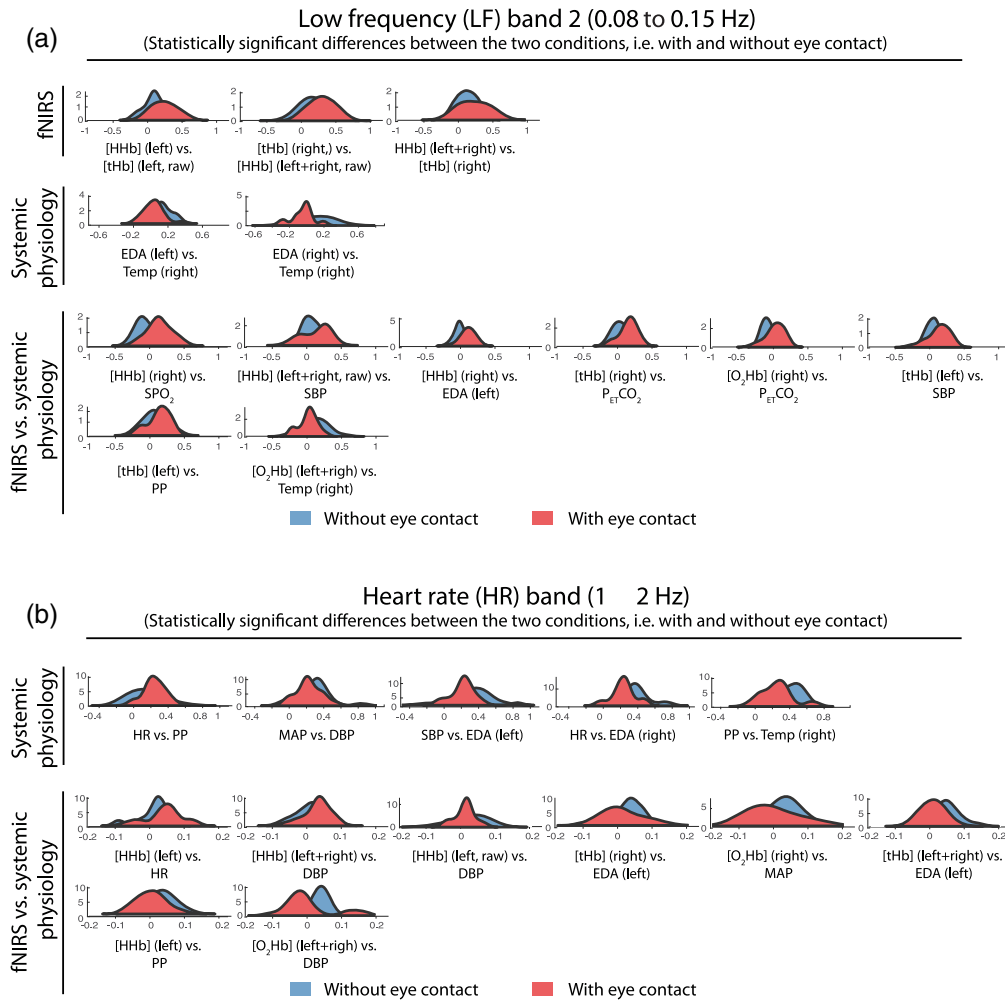


Fig. 8 Probability density functions of the distributions of each correlation coefficient of the 24 pairs in (a) the LF1 and (b) HR band separated into three groups: fNIRS, physiological, and fNIRS-physiological data. The probability density functions relative to the eye-contact condition are shown in red and those relative to the eyes-closed condition in blue. In the above figure are reported only the significant differences as a result of the Kolmogorov–Smirnov test.

in the LF2 band ($p = 0.006$). The same effect (coherence familiar pairs > coherence unfamiliar pairs) was evident in DBP and HR (VLF band, $p = 0.014$ and $p = 0.008$, respectively) and in Temp (left) (HR band, $p = 0.015$). The synchrony between the unfamiliar pairs was higher than the other one for $P_{ET}CO_2$ (LF2 band, $p = 0.019$; VLF band, $p = 0.022$), EDA (right) (HR band, $p = 0.045$), and SBP (HR band, $p = 0.026$).

3.1.3 Relation between the experimental conditions and the two groups

The statistically significant results without applying the FDR correction considering the two factors interaction (condition and group) is visualized in Fig. 11. In all the signals, the familiar pair group always shows a higher coherence during the eye contact compared with the eyes-closed condition coherence. In addition, the difference between eye-contact and eyes-closed conditions in the familiar pairs is statistically higher than the difference between the eye-contact and eyes-closed conditions in the unfamiliar pairs. No significant effect was found after performing the FDR correction. The posthoc statistics of the significant results are available in Table S3 in the [Supplemental Materials](#).

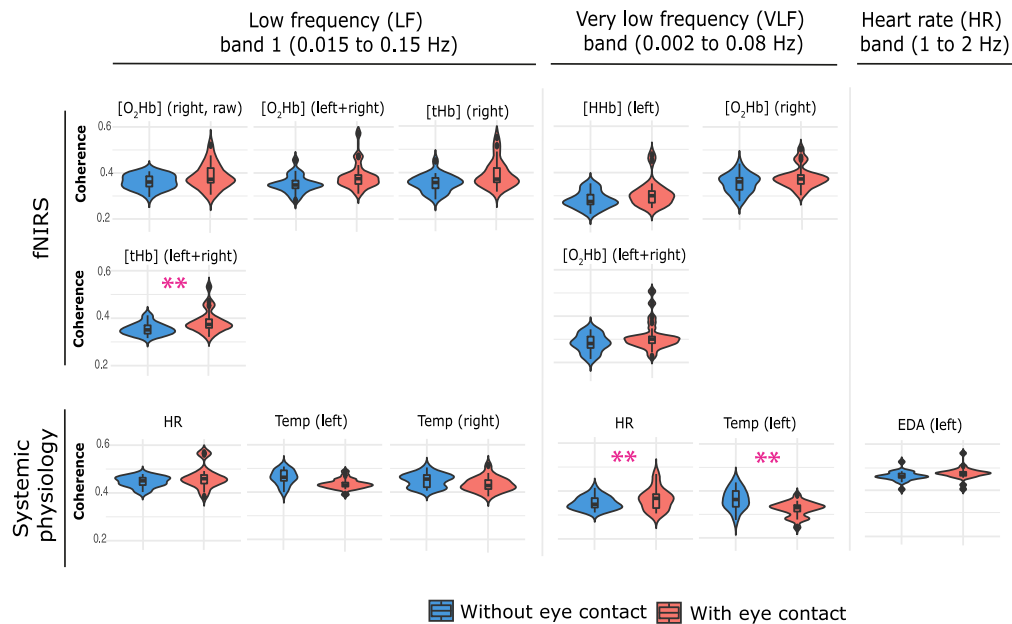


Fig. 9 Violin plots of the distributions of the WTC values over the two conditions separated into three frequency bands (LF1, VLF, and HR) and two groups: fNIRS and systemic physiology signals. In the above figure are reported only the significant differences as a result of the ART ANOVA. Double magenta asterisks refer to statistically significant differences between the two conditions even after FDR correction.

3.1.4 Control analysis

The fNIRS results of the control analysis are summarized in Table S4 in the [Supplemental Materials](#), while the systemic physiology results are listed in Table S5 in the [Supplemental Materials](#). After performing the FDR correction, our results revealed that the coherence in the real pairs were statistically higher than the spurious coherence during the eye-contact condition in many fNIRS signals: [HHb] (left), [O₂Hb] (right), [O₂Hb] (left + right), [tHb] (right), and [tHb] (left + right) in the LF1, LF2, and VLF band ($p < 0.001$); [HHb] (left, raw) in the LF1 band ($p < 0.001$), in the LF2 band ($p = 0.016$), in the VLF band ($p = 0.013$); [HHb] (right) in LF1 and VLF ($p = 0.001$); [HHb] (left + right) in LF1 and VLF ($p < 0.001$), in LF2 ($p = 0.009$); [HHb] (left + right, raw) in VLF ($p < 0.001$); [O₂Hb] (left) in LF1 and VLF ($p < 0.001$), in LF2 ($p = 0.013$); [tHb] (left) in LF1 ($p < 0.001$), in LF2 ($p = 0.001$) and in VLF ($p = 0.002$). The same effect (coherence in the real pairs > spurious coherence) was found during the eyes-closed condition: [HHb] (left) and [HHb] (left + right) in LF1 band ($p < 0.001$); [HHb] (left + right) in ($p = 0.015$); [O₂Hb] (left + right) in LF2 band ($p = 0.004$). The results confirm that coherence values in real pairs are statistically higher than those of random pairs in many fNIRS signals.

Regarding systemic physiology signals, there was a significant effect (real coherence > spurious coherence) in HR and EDA (left and right) but only before performing FDR correction.

3.2 Correlated-Coherence Coupling Analysis

3.2.1 Correlations between fNIRS and systemic physiological signals

The median correlation matrices relative to the eyes-closed and eyes-open conditions are shown in Fig. 4 (for the VLF and LF1 frequency bands) and Fig. 5 (for the LF2 and HR frequency bands). From the figures it is obvious that a strong correlation exists between all signals in the VLF band, and a higher correlation between the fNIRS signals in the other three frequency bands compared with the systemic physiology variables and fNIRS-systemic physiology variables.

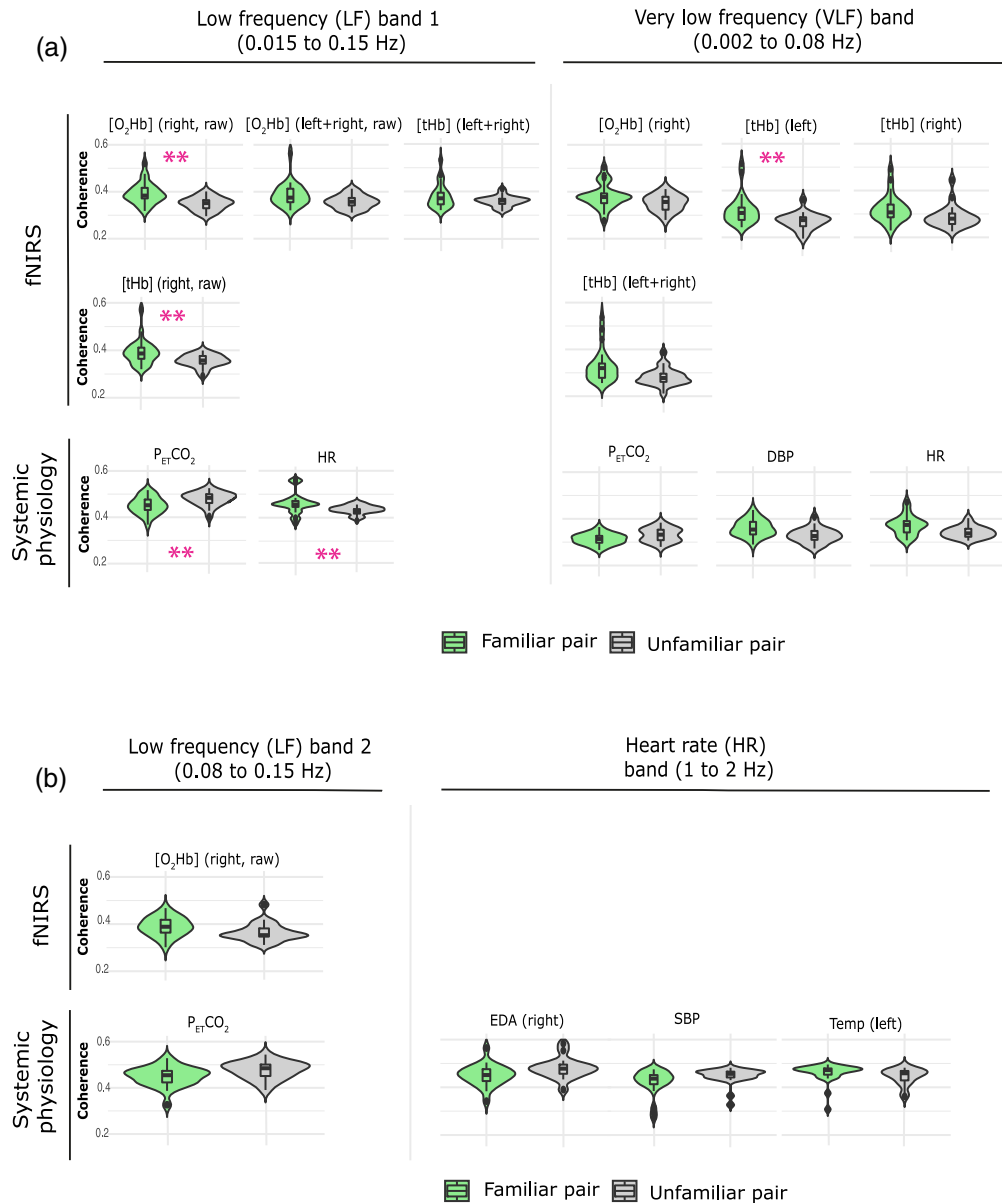


Fig. 10 Violin plots of the WTC values distributions over the two groups (familiar and unfamiliar pair) grouped into fNIRS and systemic physiology signals and separated into (a) LF1 and VLF bands and (b) LF2 and HR bands. In the above figures are reported only the significant differences as a result of the aligned ranks transformation ANOVA. Double magenta asterisks refer to statistically significant differences between the two conditions even after FDR correction.

The significant results obtained after performing the Kolmogorov–Smirnov test are grouped into three categories (fNIRS, systemic physiology and fNIRS/systemic physiology) and are illustrated in Fig. 6 (VLF band), Fig. 7 (LF1 band), and Fig. 8 (LF2 and HR bands). Statistically significant results after performing an FDR correction were marked with an asterisk.

The probability density functions of the distributions relative to the eye-contact condition are shown in red and those relative to the eyes-closed condition in blue.

The analysis framework enables us to investigate the simultaneous correlation of two time-dependent coherence vectors $[WTCS_1(t)$ and $WTCS_2(t)$, where S_1 and S_2 represent two bio-signals] between two individuals in each frequency band. A high correlation between the two coherence vectors can be indicated either as a positive time correlation between S_1 and S_2 time series or as a negative one. This method provides a synchrony indication between two pairs of signals. The correlated-coherence coupling analysis was conducted in MATLAB[®].

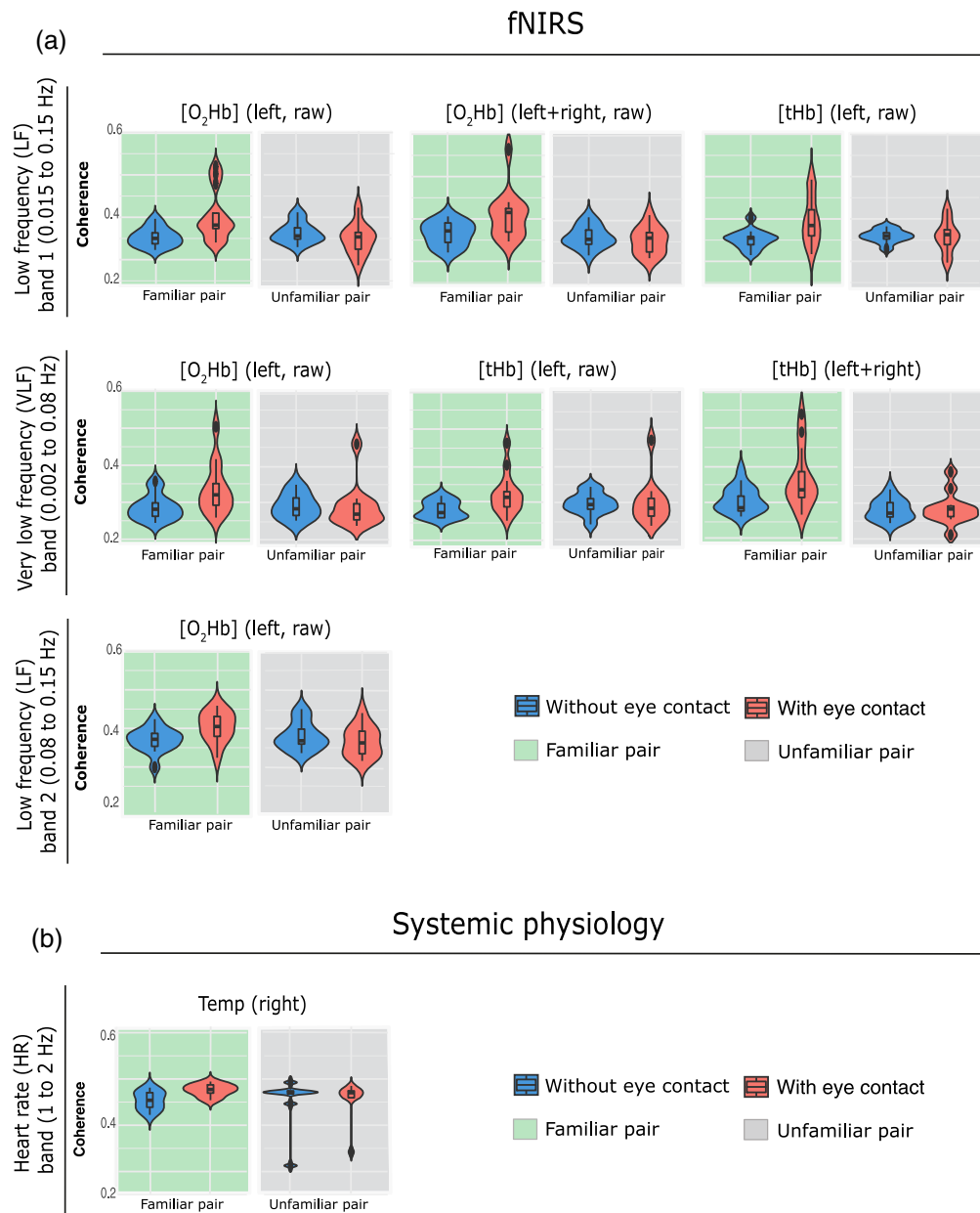


Fig. 11 Violin plots of the WTC values distributions over the two groups (familiar and unfamiliar pair) grouped into fNIRS and systemic physiology signals and separated into (a) LF1 and VLF bands and (b) LF2 and HR bands. In the above figures are reported only the significant differences as a result of the aligned ranks transformation ANOVA.

The correlation between fNIRS and systemic physiological time series was also assessed with respect to the familiar and unfamiliar pairs. The median correlation matrices relative to the pair groups are shown in Fig. S1 (for the VLF and LF1 frequency bands) and Fig. S2 (for the LF2 and HR frequency bands) in the [Supplemental Materials](#). No statistically significant difference was found between the two groups after performing FDR correction.

4 Discussion

The main goal of this study was to explore the possibility of extending the conventional fNIRS hyperscanning approach by introducing the new SPA-fNIRS hyperscanning method enabling

to simultaneously assess the brain and body synchrony from two individuals during a task involving subjects that sit in front of each other while phases of having the eyes closed and open. To investigate this, we measured changes in systemic physiology and fNIRS signals while they kept their eyes closed for 10 min and while they maintained eye contact for 10 min. We intentionally used the eyes-closed condition to ensure that the visual communication channel was totally blocked, while the prolonged eye contact was explicitly chosen to capture a strong visual interaction flow and enhance the effect of the visual channel. We also aimed to investigate the temporal relationship between the brain and body by determining the coherence between physiological, fNIRS and fNIRS/physiological signals, and we examined the role played by the visual communication channel. Previous studies have evaluated such relationships between brain activity and systemic parameters on the intrapersonal level (single brain recording),^{62–66} but we are the first that also evaluated the interpersonal level. The LF1 band (i.e. 0.015–0.15 Hz) has been identified as the frequency band in which the visual channel evokes the strongest correlation between fNIRS and physiological data signals, while the VLF band (i.e. 0.002–0.08 Hz) exhibited the highest correlation between physiological signals, as shown in Fig. 6.

Our study is the first published SPA-fNIRS hyperscanning study and the first that explores the role of eye contact for functional connectivity between the brain and the body of two individuals.

Our study shows that making eye contact for a prolonged time causes significant changes in brain-to-brain, brain-to-body, and body-to-body coupling, indicating that eye contact is followed by entrainment of the physiology between subjects. Subjects that knew each other generally showed a larger trend to change between the two conditions.

4.1 Coherence Coupling Analysis

4.1.1 Differences between eyes closed and open

Several studies have explored the importance of visual contact in social cognition so far, e.g., the importance of social attention.^{67–69} Within this context, a number of studies were performed using static images or schematic stimuli.^{70–72} Recent studies focused on face-to-face gaze rather than traditional stimulations by photo/video display.

Our study results show that pairs exhibit statistically higher coherence in physiological and fNIRS signals during face-to-face eye gaze than when their eyes were closed. Although external factors such as light coming into participants' eyes during the eye-contact phase might cause an effect on the brain and body activity, coupling between the subjects occurred at different times when they made eye contact (as also shown in Fig. 2). Therefore, we believe that the main effect is due to the visual interaction of the subjects. A strong hyperconnectivity in [tHb] in the LF1 band of the whole prefrontal cortex was found. Since for this signal the coherence in true pairs (during the eye contact) was found to be statistically higher than the coherence in random pairs, we can conclude that it is associated with social interaction. Moreover, interbody synchrony of the HR during eye contact was observed. In the VLF band, a significant and strong coherence was observed during visual communication in the skin temperature of the left wrist and the HR. In line with our results, such synchronization in HR has already been found between mother and child during face-to-face interaction.⁷³ However, since interbody synchrony in true pairs is not statistically higher than the random pairs (but only before performing the FDR correction), we cannot conclude that this effect is caused by eye contact.

Furthermore, a significant coherence during the phase of eye contact between the subjects was found in the skin temperature from both the wrists (in the LF1 band) and in EDA measured on the left wrist (in the HR band) that was not significant after the FDR correction. Concerning EDA, a similar result has been found by Jarick and Bencic⁷⁴ where dyads showed an increase in skin conductance while making eye contact compared with nondirect eye contact. To the best of our knowledge, skin temperature is a parameter has never been investigated in a hyperscanning study before.

In addition, pairwise synchrony in the eye-contact condition compared with the eyes-closed condition was also significantly greater but only without FDR correction in [O₂Hb] throughout the whole prefrontal cortex (in the VLF band) and in [tHb] in the right prefrontal cortex (in the

LF1 band). In line with our results, other studies involving the brain activity of a single subject demonstrated a difference between resting-state brain activity and brain activity when the subject was observing.^{75–89}

A few fNIRS hyperscanning studies were conducted so far that investigated the difference in functional hyperconnectivity between the eyes open and eyes closed condition. Osaka et al.⁹⁰ demonstrated a higher brain-to-brain coherence during a cooperative humming task during eye contact compare to no eye contact. Hirsch et al.⁹¹ found in the left frontal region a higher hyperconnectivity during the eye-to-eye contact compared with the eye-to-picture gaze condition.

Consistently with previous studies, the results of our study indicate that visual contact is a salient component and plays a key role in social interaction during which high hyperconnectivity was observed.

4.1.2 Relation between the experimental conditions and the two groups

The familiar group exhibited a stronger body-to-body coupling with regard to HR (in the LF1 band) and brain-to-brain coupling in terms of [tHb] of the right prefrontal region (in the VLF band) and the raw [O₂Hb] of the right prefrontal region (in the LF2 band) compared with the unfamiliar pairs. On the other hand, the unfamiliar pairs showed a stronger body-to-body coupling in terms of P_{ET}CO₂ (in the LF1 band) compared with the familiar pairs. These findings are unique.

A higher body-to-body coupling trend in the familiar group also emerged between systemic physiology variables such as EDA and skin temperature but only without FDR correction.

Slovák et al.⁹² explored the connection between EDA and emotional engagement during a conversation task. According to their findings, the degree of synchrony between pairs depends on the strength of the empathic connection between the subjects.

The familiar group exhibited a stronger synchrony trend during eye contact than the other group in terms of skin temperature (in the HR band), [O₂Hb], and [tHb]. The lack of a statistical significance may be due to the small sample size and large variability within each group.

4.2 Correlated-Coherence Coupling Analysis

4.2.1 Higher coherence during eye contact between physiological data

We found a significantly higher coherence between skin temperature (from both wrists) and EDA in the VLF band when the subjects had eye contact compared to the period when they had their eyes closed even after the FDR correction. EDA changes depend on the quantity of sweat secreted by eccrine sweat glands controlled by the sympathetic nervous system (SNS). If the sympathetic branch of the autonomic nervous system (ANS) is highly activated, the sweat glands activity increases, leading to higher skin conductance, and vice versa. Previous studies have shown that eye contact leads to significantly higher skin conductance compared with nonmutual gaze.^{93–97} The relationship between EDA, skin temperature, and mutual gaze has never before been investigated. Khan et al.⁹⁸ reported results similar to ours, noting a significant positive correlation between these two variables when students performed an engineering exam. The higher correlation of two pairs EDA time series during eye contact could be attributable to an increased emotional response either as a result of affection or due to a sense of unease. This increased the EDA and the skin conductance. On the other hand, this could trigger cutaneous vasoconstriction, which results in decreased skin blood flow inducing a drop in skin temperature. In fact, skin temperature is directly correlated with peripheral blood flow.⁹⁹ Based on this, recent studies have shown that direct eye contact between two people causes a stress reaction, which manifests itself as an increased SNS activity.¹⁰⁰ As a result, the high correlation during the eyes open condition between EDA and Temp coherence vectors may be attributable to a negative time correlation between the two signals of the individual pairs.

The same pattern was observed between the skin temperature of the left wrist and P_{ET}CO₂ in the VLF band as well as between the skin temperature of the right wrist and P_{ET}CO₂ in the LF1 band. An increase in P_{ET}CO₂ coherence between pairs may theoretically arise from three sources: simultaneous decrease (or increase) in alveolar ventilation, increase (or decrease)

in CO₂ production, and the quantity of CO₂ that contributes to the respiratory capillary circulation.¹⁰¹ Respiratory reactions induced by eye contact produce changes in ventilation that are reflected by alterations in P_{ET}CO₂. In fact, in most people, emotional arousal is linked to reduced P_{ET}CO₂ levels.¹⁰² This slight hypocapnia occurs when alveolar ventilation is greater than that required to eliminate metabolically formed CO₂.¹⁰³ Since the arousal affects both parameters simultaneously, this leads to a high coherence.

Significant coherence was found in the VLF and LF1 band between the skin temperature (of both wrists) and cardiovascular variables such as HR, PP, SBP, SpO₂ and MAP. Such cardiovascular variations may be interpreted as an SNS response related to the pair's interaction.¹⁰⁴

In addition, a significant symmetry in both wrists between EDAs as well as skin temperatures was found in the VLF band. In the LF1 band instead, coherence in P_{ET}CO₂ was found to be correlated to the coherence in PP (also after the FDR correction) and SBP.

In fact, during eye contact, the cardiovascular variables are affected by the ANS. Both branches of the ANS (parasympathetic nervous system and SNS) are of significant importance in controlling cardiovascular dynamics, including HR, MAP regulation, and respiration,^{105,106} but they have contrary effects on the functions they regulate. In case of possible discomfort, due to the mutual gaze of the pairs, the SNS is more activated, causing an increase in MAP and, at the same time, in skin conductance.

Several studies have investigated and found an asymmetry between the right and left sides of the human body related to the measurement of skin temperature and EDA.¹⁰⁷⁻¹¹⁰ These results could explain the reason why some variables in our study are correlated only with EDA and/or skin temperatures on the right wrist and not on the left and vice versa. Besides, this relationship was found to be stronger on the right wrist in accordance with Demirel et al.¹⁰⁷ According to Demirel et al., such asymmetry may be associated with the peripheral immune asymmetry or asymmetric lymph node distribution.

In our results, skin temperature plays a predominant role. In fact, correlations with several cardiovascular and EDA parameters have been found, and most importantly, the correlation during eye contact has been found to be more significant than that period when the subject had their eyes closed.

4.2.2 Higher coherence during eye contact between physiological and fNIRS data

Several significant temporal relationships between fNIRS and systemic physiological signals were identified, mainly in the LF1 (see Fig. 7). This is an indicator that the fNIRS signal was influenced by changes in systemic physiology.^{42,46,111,112} The fNIRS signals measured therefore represent a weighted sum of physiological changes due to neurovascular coupling as well as due to different physiological causes (e.g. changes in systemic physiology).

The strong coherence in all frequency bands between fNIRS signals and EDA is the most prominent finding. This is in line with previous publications that focused on investigating a relationship between brain hemodynamics and oxygenation with EDA on the intrapersonal level.⁶²⁻⁶⁵ This relationship was found to be dependent on the type of task the participants were involved, as discussed by Holper et al.⁶⁶

Another remarkable finding is the higher coherence in the signal phase during eye contact between skin temperature and fNIRS signals, especially in the LF1 frequency band. Concerning the skin temperature, we found an interesting pattern: While the correlation between physiological signals and skin temperature was higher in the right arm in the LF1 and VLF bands, the correlation between fNIRS signals and skin temperature in the LF1 band was predominant in the left wrist. This is a unique finding in this study.

In addition, a significant correlation between the fNIRS variable and the P_{ET}CO₂ was obtained, only for the right prefrontal region in the LF1 and LF2 bands.

Our results suggest the presence of interconnection between cerebral hemodynamic variables and SNS activity. Although such relationships have been reported previously, we are the first to identify them in investigating the long-term effects of eye contact in the context of SPA-hyperscanning.

4.2.3 Higher coherence during eye contact between fNIRS data

The strongest correlation during eye contact of fNIRS occurred in the LF1 and LF2 bands. No evident pattern has arisen apart from a greater symmetry between the left and right region in [O₂Hb] as well as in [tHb] in the LF1 band during the eye contact period compared with the period with eyes closed.

4.2.4 Higher coherence during eyes-closed condition

A lower coherence was observed in some signals in all four frequency bands during the eyes' contact than when eye contact was blocked. We have found no explanation for this phenomenon.

5 Strengths and Limitations

We are the first group to perform a SPA-fNIRS hyperscanning study capturing changes in cerebral oxygenation and hemodynamics as well as systemic physiology in two subjects in parallel. We performed an advanced signal analysis to capture the coupling of the signals in the time-frequency domain within and between the two subjects, and we had enough subjects to perform a subgroup analysis enabling us to find differences in the coupling between pairs of subjects according to their relationship.

Our experimental study allowed us to test the feasibility of our novel framework and to prove that, with a simple experimental design, it is already possible to identify significant changes in biosignals that have not been investigated in detail in previous studies (using fNIRS or fMRI). There are many possible extensions to our data analysis. For example, cross-frequency coupling could also be examined in the future.

Although our primary focus was to assess the influence of the visual communication channel, an interesting step in the further investigation might be to consider a third condition, in which participants keep their eyes open without making eye contact, to exclude that part of the effect might be due only by the difference between eyes-open versus eyes-closed conditions.

It should be pointed out that, although in everyday life there are scenarios in which prolonged eye contact plays an important role in social interaction (e.g., the conversation between friends, couples, and interviews), keeping eye contact for 10 min something that happens rather rarely in everyday life.

A limitation of our approach might be the lack of an eye-tracking system in our setup and, therefore, a precise temporal indication of when eye contact occurred and how long it lasted is missing. The lack of brain/body coupling we found for specific individuals may be associated, not only with how subjects are related but also with too short a gaze to achieve brain-to-brain and body-to-body synchrony, due to the greater discomfort perceived by one person in staring into the eyes of another person.

Within this context, automatic identification of a subset of relevant features for each pair is crucial for a robust building of a synchronization model, which considers actual eye contact. The difference between the cross-brain correlations of the two groups is attributable to the participants' relationships. Individuals who know each other well connect with a higher empathy. This assumption might be addressed in future studies exploring brain and body synchrony of different groups such as mother-child and nurse-child.

6 Conclusions

The main goal of this exploratory study was to provide a new framework for assessing brain-to-brain, brain-to-body, and body-to-body coupling between interacting subject pairs that can be adopted in future hyperscanning studies. To give an example of our novel SPA-fNIRS hyperscanning approach, we tested it on a simple social experimental paradigm while enabling or disabling visual communication between the subject pairs.

We found by the coherence coupling analysis that the eye contact generally causes an increase in brain-to-brain coupling (e.g., [tHb] in the LF1 band) and characteristic changes

in the body-to-body coupling (e.g., an increase of the HR in the VLF band a decrease in the temperature of the left wrist also in the VLF band). The changes due to the eye contact showed a relationship-dependent trend, i.e., pairs that were well acquainted with each other showed a higher increase in brain-to-brain coupling (in the LF and VLF bands) and an increase/decrease in body-to-body coupling (with regard to $P_{ET}CO_2$ and HR in the LF band, respectively) compared with the phase without eye contact. Our correlated-coherence coupling analysis revealed complex changes in the correlation of coupling changes between several brain and body-related physiological signals.

Our study shows that looking at each other for a prolonged time causes significant changes in brain-to-brain, brain-to-body, and body-to-body coupling, indicating that looking at each other is accompanied by entrainment of the physiology between subjects. This has implications for all life situations where eye-to-eye contact is happening for a prolonged time, e.g., during a teaching situation (pupils versus teacher and students versus lecturer) or a dialogue (e.g., interview, psychological consultation, or team meeting).

Our study is also the first that employed the SPA-fNIRS approach and showed its usefulness to investigate complex interpersonal physiological changes. We recommend for future fNIRS hyperscanning studies to also use the SPA-fNIRS approach since it provides much more information and insights into the physiological coupling between subjects compared with the classical fNIRS approach that only focuses on the brain. Both the brain and the body coupling need to be assessed to have a comprehensive understanding of physiological changes associated with social cognition. SPA-fNIRS has a great potential for social neuroscience to explore physiological couplings in various real-life conditions and circumstances.

Disclosures

The authors declare no potential conflicts of interest with respect to the research, authorship, and/or publication of this article. F. Scholkmann consulted for NIRx Medizintechnik GmbH (Berlin, Germany) on an unrelated subject matter. M. Wolf is president of the board and cofounder of OxyPrem AG.

Acknowledgments

This research was funded by the Swiss National Science Foundation (Grant No. 159490). The study was conducted according to the guidelines of the Declaration of Helsinki, and approved by the Ethics Committee of the County of Zurich (KEK-ZH-Nr. E50/2002 of 12/20/2013). We thank our students for their contribution to the measurements and our subjects for participating in this study funding.

Code, Data, and Materials Availability

The data are not publicly available due to legal and ethical reasons.

References

1. “The cooperative human,” *Nat. Hum. Behav.* **2**(7), 427–428 (2018).
2. A. I. Goldman, “Précis of simulating minds: the philosophy, psychology, and neuroscience of mindreading,” *Philos. Stud.* **144**(3), 431–434 (2009).
3. V. Gallese, “Embodied simulation: from neurons to phenomenal experience,” *Phenomenol. Cognit. Sci.* **4**(1), 23–48 (2005).
4. P. Nystrom, “The infant mirror neuron system studied with high density EEG,” *Soc. Neurosci.* **3**(3–4), 334–347 (2008).
5. S. Shimada and K. Hiraki, “Infant’s brain responses to live and televised action,” *NeuroImage* **32**(2), 930–939 (2006).
6. T. Singer and C. Lamm, “The social neuroscience of empathy,” *Ann. N. Y. Acad. Sci.* **1156**, 81–96 (2009).

7. M. L. Meyer et al., "Empathy for the social suffering of friends and strangers recruits distinct patterns of brain activation," *Soc. Cognit. Affect Neurosci.* **8**(4), 446–454 (2013).
8. K. Jankowiak-Siuda, K. Rymarczyk, and A. Grabowska, "How we empathize with others: a neurobiological perspective," *Med. Sci. Monit.* **17**(1), RA18–RA24 (2011).
9. B. Wicker et al., "Both of us disgusted in My insula: the common neural basis of seeing and feeling disgust," *Neuron* **40**(3), 655–664 (2003).
10. C. I. Hooker et al., "Mentalizing about emotion and its relationship to empathy," *Soc. Cognit. Affect Neurosci.* **3**(3), 204–217 (2008).
11. C. Keysers et al., "A touching sight: SII/PV activation during the observation and experience of touch," *Neuron* **42**(2), 335–346 (2004).
12. L. J. Carver and B. G. Vaccaro, "12-month-old infants allocate increased neural resources to stimuli associated with negative adult emotion," *Dev. Psychol.* **43**(1), 54–69 (2007).
13. N. Kanwisher, J. McDermott, and M. M. Chun, "The fusiform face area: a module in human extrastriate cortex specialized for face perception," *J. Neurosci.* **17**(11), 4302–4311 (1997).
14. N. Sebanz, H. Bekkering, and G. Knoblich, "Joint action: bodies and minds moving together," *Trends Cognit. Sci.* **10**(2), 70–76 (2006).
15. T. Liu, H. Saito, and M. Oi, "Role of the right inferior frontal gyrus in turn-based cooperation and competition: a near-infrared spectroscopy study," *Brain Cognit.* **99**, 17–23 (2015).
16. S. N. Young, "The neurobiology of human social behaviour: an important but neglected topic," *J. Psychiatr. Neurosci.* **33**(5), 391–392 (2008).
17. F. Babiloni and L. Astolfi, "Social neuroscience and hyperscanning techniques: past, present and future," *Neurosci. Biobehav. Rev.* **44**, 76–93 (2014).
18. M. Balconi and M. E. Vanutelli, "Cooperation and competition with hyperscanning methods: review and future application to emotion domain," *Front. Comput. Neurosci.* **11**, 86 (2017).
19. A. Czeszumski et al., "Hyperscanning: a valid method to study neural inter-brain underpinnings of social interaction," *Front. Hum. Neurosci.* **14**, 39 (2020).
20. G. Dumas, "Towards a two-body neuroscience," *Commun Integr. Biol.* **4**(3), 349–352 (2011).
21. G. Dumas et al., "From social behaviour to brain synchronization: Review and perspectives in hyperscanning," *IRBM* **32**(1), 48–53 (2011).
22. A. Gevins, C. S. Chan, and L. Sam-Vargas, "Towards measuring brain function on groups of people in the real world," *PLoS One* **7**(9), e44676 (2012).
23. M. Y. Wang et al., "Concurrent mapping of brain activation from multiple subjects during social interaction by hyperscanning: a mini-review," *Quant Imaging Med. Surg.* **8**(8), 819–837 (2018).
24. P. R. Montague et al., "Hyperscanning: simultaneous fMRI during linked social interactions," *NeuroImage* **16**(4), 1159–1164 (2002).
25. L. Astolfi et al., "Investigating the neural basis of empathy by EEG hyperscanning during a Third Party Punishment," in *Annu. Int. Conf. IEEE Eng. Med. Biol. Soc.*, pp. 5384–5387 (2015).
26. J. C. Fachner et al., "'Telling me not to worry...' hyperscanning and neural dynamics of emotion processing during guided imagery and music," *Front. Psychol.* **10**, 1561 (2019).
27. L. Holper, F. Scholkmann, and M. Wolf, "Between-brain connectivity during imitation measured by fNIRS," *NeuroImage* **63**(1), 212–222 (2012).
28. X. Cui, D. M. Bryant, and A. L. Reiss, "NIRS-based hyperscanning reveals increased interpersonal coherence in superior frontal cortex during cooperation," *NeuroImage* **59**(3), 2430–2437 (2012).
29. T. Funane et al., "Synchronous activity of two people's prefrontal cortices during a cooperative task measured by simultaneous near-infrared spectroscopy," *J. Biomed. Opt.* **16**(7), 077011 (2011).
30. L. Astolfi et al., "Neuroelectrical hyperscanning measures simultaneous brain activity in humans," *Brain Topogr.* **23**(3), 243–256 (2010).

31. F. Babiloni et al., “High resolution EEG hyperscanning during a card game,” in *29th Annu. Int. Conf. IEEE Eng. Med. and Biol. Soc.*, pp. 4957–4960 (2007).
32. F. Babiloni et al., “Simultaneous tracking of multiple brains activity with high resolution EEG hyperscannings,” in *Joint Meeting 6th Int. Symp. Noninvasive Functional Source Imaging Brain and Heart and Int. Conf. Funct. Biomed. Imaging*, pp. 196–199 (2007).
33. F. Babiloni et al., “Hypermethods for EEG hyperscanning,” in *Conf. Proc. IEEE Eng. Med. Biol. Soc.*, pp. 3666–3669 (2006).
34. D. Liu et al., “Interactive brain activity: review and progress on EEG-based hyperscanning in social interactions,” *Front. Psychol.* **9**, 1862 (2018).
35. P. Pinti et al., “The present and future use of functional near-infrared spectroscopy (fNIRS) for cognitive neuroscience,” *Ann. N. Y. Acad. Sci.* **1464**(1), 5–29 (2020).
36. P. Pinti et al., “A review on the use of wearable functional near-infrared spectroscopy in naturalistic environments(,)” *Jpn. Psychol. Res.* **60**(4), 347–373 (2018).
37. F. Scholkmann et al., “A review on continuous wave functional near-infrared spectroscopy and imaging instrumentation and methodology,” *NeuroImage* **85**(Pt 1), 6–27 (2014).
38. L. Dommer et al., “Between-brain coherence during joint n-back task performance: a two-person functional near-infrared spectroscopy study,” *Behav. Brain Res.* **234**(2), 212–222 (2012).
39. F. Scholkmann et al., “A new methodical approach in neuroscience: assessing inter-personal brain coupling using functional near-infrared imaging (fNIRI) hyperscanning,” *Front Hum Neurosci* **7**, 813 (2013).
40. A. F. d. C. Hamilton, “Hyperscanning: beyond the hype,” *Neuron* **109**, 404–407 (2021).
41. I. Tachtsidis and F. Scholkmann, “False positives and false negatives in functional near-infrared spectroscopy: issues, challenges, and the way forward,” *Neurophotonics* **3**(3), 030401 (2016).
42. M. Caldwell et al., “Modelling confounding effects from extracerebral contamination and systemic factors on functional near-infrared spectroscopy,” *NeuroImage* **143**, 91–105 (2016).
43. I. Tachtsidis and A. Papaioannou, “Investigation of frontal lobe activation with fNIRS and systemic changes during video gaming,” *Adv. Exp. Med. Biol.* **789**, 89–95 (2013).
44. I. Tachtsidis et al., “Investigation of frontal cortex, motor cortex and systemic haemodynamic changes during anagram solving,” *Adv. Exp. Med. Biol.* **614**, 21–28 (2008).
45. F. Scholkmann et al., “End-tidal CO₂: an important parameter for a correct interpretation in functional brain studies using speech tasks,” *NeuroImage* **66**, 71–79 (2013).
46. F. Scholkmann, M. Wolf, and U. Wolf, “The effect of inner speech on arterial CO₂ and cerebral hemodynamics and oxygenation: a functional NIRS study,” *Adv. Exp. Med. Biol.* **789**, 81–87 (2013).
47. H. Zohdi, F. Scholkmann, and U. Wolf, “Frontal cerebral oxygenation asymmetry: inter-subject variability and dependence on systemic physiology, season, and time of day,” *Neurophotonics* **7**(2), 025006 (2020).
48. F. Scholkmann et al., “Effect of short-term colored-light exposure on cerebral hemodynamics and oxygenation, and systemic physiological activity,” *Neurophotonics* **4**(4), 045005 (2017).
49. A. J. Metz et al., “Continuous coloured light altered human brain haemodynamics and oxygenation assessed by systemic physiology augmented functional near-infrared spectroscopy,” *Sci. Rep.* **7**(1), 10027 (2017).
50. M. A. Yücel et al., “Best practices for fNIRS publications,” *Neurophotonics* **8**(1), 012101 (2021).
51. J. R. Goodwin, C. R. Gaudet, and A. J. Berger, “Short-channel functional near-infrared spectroscopy regressions improve when source–detector separation is reduced,” *Neurophotonics* **1**(1), 015002 (2014).
52. S. Brigadoi and R. J. Cooper, “How short is short? Optimum source-detector distance for short-separation channels in functional near-infrared spectroscopy,” *Neurophotonics* **2**(2), 025005 (2015).
53. M. A. Yücel et al., “Short separation regression improves statistical significance and better localizes the hemodynamic response obtained by near-infrared spectroscopy for tasks with differing autonomic responses,” *Neurophotonics* **2**(3), 035005 (2015).

54. R. B. Saager and A. J. Berger, "Direct characterization and removal of interfering absorption trends in two-layer turbid media," *J. Opt. Soc. Am. A* **22**(9), 1874–1882 (2005).
55. F. Scholkmann, A. J. Metz, and M. Wolf, "Measuring tissue hemodynamics and oxygenation by continuous-wave functional near-infrared spectroscopy—how robust are the different calculation methods against movement artifacts?" *Physiol. Meas.* **35**(4), 717–734 (2014).
56. J. S. Wyatt et al., "Quantification of cerebral oxygenation and haemodynamics in sick newborn infants by near infrared spectrophotometry," *Lancet* **328**(8515), 1063–1066 (1986).
57. P. Pinti et al., "The role of anterior prefrontal cortex (area 10) in face-to-face deception measured with fNIRS," *Soc. Cognit. Affect Neurosci.* **16**(1-2), 129–142 (2021).
58. N. Kollias and W. Gratzer, "Tabulated molar extinction coefficient for hemoglobin in water," Wellman Laboratories, Harvard Medical School, Boston, Vol. 5, pp. 150–161 (1999).
59. G. A. Zimeo Morais et al., "Non-neuronal evoked and spontaneous hemodynamic changes in the anterior temporal region of the human head may lead to misinterpretations of functional near-infrared spectroscopy signals," *Neurophotonics* **5**(1), 011002 (2018).
60. A. Grinsted, J. C. Moore, and S. Jevrejeva, "Application of the cross wavelet transform and wavelet coherence to geophysical time series," *Nonlinear Processes. Geophys.* **11**(5/6), 561–566 (2004).
61. J. O. Wobbrock et al., "The aligned rank transform for nonparametric factorial analyses using only anova procedures," in *Proc. SIGCHI Conf. Human Factors Comput. Syst.*, Association for Computing Machinery, Vancouver, BC, Canada, pp. 143–146 (2011).
62. M. Fredrikson et al., "Functional neuroanatomical correlates of electrodermal activity: a positron emission tomographic study," *Psychophysiology* **35**(2), 179–185 (1998).
63. M. Gamer et al., "fMRI-activation patterns in the detection of concealed information rely on memory-related effects," *Soc. Cognit. Affect Neurosci.* **7**(5), 506–515 (2012).
64. M. K. Park, N. Satoh, and M. Kumashiro, "Mental workload under time pressure can trigger frequent hot flashes in menopausal women," *Ind. Health* **46**(3), 261–268 (2008).
65. L. M. Williams et al., "BOLD, sweat and fears: fMRI and skin conductance distinguish facial fear signals," *Neuroreport* **16**(1), 49–52 (2005).
66. L. Holper, F. Scholkmann, and M. Wolf, "The relationship between sympathetic nervous activity and cerebral hemodynamics and oxygenation: a study using skin conductance measurement and functional near-infrared spectroscopy," *Behav. Brain Res.* **270**, 95–107 (2014).
67. V. Corkum and C. Moore, "The origins of joint visual attention in infants," *Dev. Psychol.* **34**(1), 28–38 (1998).
68. T. Farroni et al., "Eye contact detection in humans from birth," *Proc. Natl. Acad. Sci. U.S.A.* **99**(14), 9602–9605 (2002).
69. C. I. Hooker et al., "Brain networks for analyzing eye gaze," *Brain Res. Cognit. Brain Res.* **17**(2), 406–418 (2003).
70. T. Ethofer, M. Gschwind, and P. Vuilleumier, "Processing social aspects of human gaze: a combined fMRI-DTI study," *NeuroImage* **55**(1), 411–419 (2011).
71. D. N. Saito et al., "'Stay tuned': inter-individual neural synchronization during mutual gaze and joint attention," *Front. Integr. Neurosci.* **4**, 127 (2010).
72. A. Senju and M. H. Johnson, "The eye contact effect: mechanisms and development," *Trends Cognit. Sci.* **13**(3), 127–134 (2009).
73. R. Feldman et al., "Mother and infant coordinate heart rhythms through episodes of interaction synchrony," *Infant Behav. Dev.* **34**(4), 569–577 (2011).
74. M. Jarick and R. Bencic, "Eye contact is a two-way street: arousal is elicited by the sending and receiving of eye gaze information," *Front. Psychol.* **10**, 1262 (2019).
75. C. Yan et al., "Spontaneous brain activity in the default mode network is sensitive to different resting-state conditions with limited cognitive load," *PLoS One* **4**(5), e5743 (2009).
76. Q. Zou et al., "Functional connectivity between the thalamus and visual cortex under eyes closed and eyes open conditions: a resting-state fMRI study," *Hum. Brain Mapp.* **30**(9), 3066–3078 (2009).

77. J. Wei et al., “Eyes-open and eyes-closed resting states with opposite brain activity in sensorimotor and occipital regions: multidimensional evidences from machine learning perspective,” *Front. Hum. Neurosci.* **12**, 422 (2018).
78. B. Tan et al., “The difference of brain functional connectivity between eyes-closed and eyes-open using graph theoretical analysis,” *Comput. Math. Methods Med.* **2013**, 1–15 (2013).
79. A. R. Merzagora et al., “fNIR study of prefrontal cortex activity during eyes-open and eyes-closed conditions,” *NeuroImage* **47**, S142 (2009).
80. E. Marx et al., “Eyes open and eyes closed as rest conditions: impact on brain activation patterns,” *NeuroImage* **21**(4), 1818–1824 (2004).
81. R. J. Barry et al., “EEG differences between eyes-closed and eyes-open resting conditions,” *Clin. Neurophysiol.* **118**(12), 2765–2773 (2007).
82. A. C. Chen et al., “EEG default mode network in the human brain: spectral regional field powers,” *NeuroImage* **41**(2), 561–574 (2008).
83. E. Marx et al., “Eye closure in darkness animates sensory systems,” *NeuroImage* **19**(3), 924–934 (2003).
84. M. Wiesmann et al., “Eye closure in darkness animates olfactory and gustatory cortical areas,” *NeuroImage* **32**(1), 293–300 (2006).
85. H. Yang et al., “Amplitude of low frequency fluctuation within visual areas revealed by resting-state functional MRI,” *NeuroImage* **36**(1), 144–152 (2007).
86. M. McAvoy et al., “Resting states affect spontaneous BOLD oscillations in sensory and paralimbic cortex,” *J. Neurophysiol.* **100**(2), 922–931 (2008).
87. K. Hübner et al., “Differences in saccade-evoked brain activation patterns with eyes open or eyes closed in complete darkness,” *Exp. Brain Res.* **186**(3), 419–430 (2008).
88. B.-K. Yuan et al., “Amplitude differences in high-frequency fMRI signals between eyes open and eyes closed resting states,” *Front. Hum. Neurosci.* **8**, 503 (2014).
89. B. Liang et al., “Brain spontaneous fluctuations in sensorimotor regions were directly related to eyes open and eyes closed: evidences from a machine learning approach,” *Front. Hum. Neurosci.* **8**, 645 (2014).
90. N. Osaka et al., “Neural synchronization during cooperated humming: a hyperscanning study using fNIRS,” *Procedia Social Behav. Sci.* **126**, 241–243 (2014).
91. J. Hirsch et al., “Frontal temporal and parietal systems synchronize within and across brains during live eye-to-eye contact,” *NeuroImage* **157**, 314–330 (2017).
92. P. Slovák et al., “Exploring skin conductance synchronisation in everyday interactions,” in *Proc. 8th Nordic Conf. Human-Comput. Interaction: Fun, Fast, Found.*, Association for Computing Machinery, Helsinki, Finland, pp. 511–520 (2014).
93. L. Conty et al., “The mere perception of eye contact increases arousal during a word-spelling task,” *Soc. Neurosci.* **5**(2), 171–186 (2010).
94. T. M. Helminen, S. M. Kaasinen, and J. K. Hietanen, “Eye contact and arousal: the effects of stimulus duration,” *Biol. Psychol.* **88**(1), 124–130 (2011).
95. A. Mazur et al., “Physiological aspects of communication via mutual gaze,” *AJS* **86**(1), 50–74 (1980).
96. K. A. Nichols and B. G. Champness, “Eye gaze and the GSR,” *J. Exp. Social Psychol.* **7**(6), 623–626 (1971).
97. R. Soussignan et al., “Self-relevance appraisal of gaze direction and dynamic facial expressions: effects on facial electromyographic and autonomic reactions,” *Emotion* **13**(2), 330–337 (2013).
98. T. H. Khan et al., “Exploring relationships between electrodermal activity, skin temperature, and performance during,” in *IEEE Front. Educ. Conf.*, pp. 1–5 (2019).
99. R. Aaslid, “Cerebral autoregulation and vasomotor reactivity,” *Front. Neurol. Neurosci.* **21**, 216–228 (2006).
100. J. K. Hietanen et al., “Seeing direct and averted gaze activates the approach-avoidance motivational brain systems,” *Neuropsychologia* **46**(9), 2423–2430 (2008).
101. J. B. West, “State of the art: ventilation-perfusion relationships,” *Am. Rev. Respir. Dis.* **116**(5), 919–943 (1977).
102. D. L. Dudley, *Psychophysiology of Respiration in Health and Disease*, Appleton-Century-Crofts, New York (1969).

103. B. Silvestri, "Physiology of respiration 2nd ed.," *Phys. Ther.* **55**(8), 928–928 (1975).
104. T. Akata et al., "Reliability of fingertip skin-surface temperature and its related thermal measures as indices of peripheral perfusion in the clinical setting of the operating theatre," *Anaesth Intensive Care* **32**(4), 519–529 (2004).
105. N. Charkoudian and J. A. Rabbitts, "Sympathetic neural mechanisms in human cardiovascular health and disease," *Mayo Clin. Proc.* **84**(9), 822–830 (2009).
106. S. C. Malpas, "Sympathetic nervous system overactivity and its role in the development of cardiovascular disease," *Physiol. Rev.* **90**(2), 513–557 (2010).
107. H. Demirel et al., "Right-sided lateralization of skin temperature in healthy young persons," *Clin. Invest. Med.* **39**(6), 27515 (2016).
108. S. Fisher and J. Abercrombie, "The relationship of body image distortions to body reactivity gradients," *J. Pers.* **26**(3), 320–329 (1958).
109. S. Fisher and S. E. Cleveland, "Right-left body reactivity patterns in disorganized states," *J. Nerv. Ment. Dis.* **128**(5), 396–400 (1959).
110. K. Kasos et al., "Does the electrodermal system 'take sides' when it comes to emotions?" *Appl. Psychophysiol. Biofeedback* **43**(3), 203–210 (2018).
111. N. Nasser et al., "Impact of changes in systemic physiology on fNIRS/NIRS signals: analysis based on oblique subspace projections decomposition," *Adv. Exp. Med. Biol.* **1072**, 119–125 (2018).
112. U. Wolf et al., "Changes in hemodynamics and tissue oxygenation saturation in the brain and skeletal muscle induced by speech therapy—a near-infrared spectroscopy study," *Sci. World J.* **11**, 1206–1215 (2011).

Sabino Guglielmini is a doctoral student at the Department of Information Technology and Electrical Engineering at ETH Zurich, and a member of the Biomedical Optics Research Laboratory, University Hospital Zurich. He received his master's degree in computer science with a specialization in computational intelligence at the University of Salerno (UNISA, Italy), in 2018. His research focuses on biomedical signal processing, machine learning, and the use of functional near-infrared spectroscopy in hyperscanning studies.

Gino Bopp is a final-year medical student at the University of Zurich. The research at the University Hospital Zurich (Biomedical Optics Research Laboratory, Department of Neonatology) contributed to his master's thesis.

Valentine L. Marcar: biography is not available.

Felix Scholkmann received his PhD from the University of Zurich, Switzerland, in 2014. He is a lecturer at the University of Zurich and a research associate at the University Hospital Zurich (Biomedical Optics Research Laboratory, Department of Neonatology) and University of Bern. His research mainly concerns the fields of neurophotonics and biomedical signal processing, as well as integrative neuroscience and physiology.

Martin Wolf is professor of biomedical optics at University of Zurich. He completed his PhD at ETH Zurich and was a postdoc at University of Illinois at Urbana-Champaign. He is expert in near infrared spectroscopy (NIRS), optical tomography (NIROT) and functional NIRS (fNIRS) covering technological, signal analysis and application aspects.